Vol. 601: 41–57, 2018
https://doi.org/10.3354/meps12670

MARINE ECOLOGY PROGRESS SERIES
Mar Ecol Prog Ser

Published August 9

Photoinactivation, repair and the motility–physiology trade-off in microphytobenthos

Silja Frankenbach*, William Schmidt, Jörg C. Frommlet, João Serôdio

Departamento de Biologia and CESAM – Centro de Estudos do Ambiente e do Mar, Universidade de Aveiro, Campus de Santiago, 3810-193 Aveiro, Portugal

ABSTRACT: Microphytobenthos (MPB) inhabiting intertidal flats of estuaries form highly productive diatom-dominated biofilms. The capacity to sustain such high photosynthetic activity under conditions prone to cause photoinhibition is thought to be enabled by efficient photoprotective mechanisms, the main ones being the xanthophyll cycle (XC) and vertical migration (VM). This study compared the photoprotective capacity of 2 MPB communities inhabiting contrasting sedimentary habitats and relying on distinct light responses: epipelic communities, colonizing muddy sediments and using motility (VM) to regulate light exposure; and epipsammic communities, inhabiting sandier sediments and relying solely on physiological photoprotection (XC). The efficiency of physiological photoprotection of the 2 communities was compared regarding Photosystem II (PSII) photoinactivation caused by light stress. Lincomycin was used to distinguish photoinactivation from counteracting repair. Rate constants of PSII photoinactivation (k_{PI}) and repair (k_{REC}) were determined on cell suspensions, based on the light and time dependence of maximum quantum yield of PSII, F_v/F_m, as measured using multi-actinic imaging fluorometry. The results show that motile species, in comparison to epipsammic ones, are inherently more susceptible to photoinactivation (higher k_{PI}), less dependent on the XC for preventing photodamage (smaller increase of k_{PI} induced by nigericin) and more efficient regarding repair capacity (higher k_{REC}). The distinct strategies exhibited by epipelic and epipsammic communities to cope with light stress support the hypothesized trade-off between photoprotective motility and photophysiology. Motile forms have a diminished physiological capacity for preventing photodamage and compensate using VM and a better repair capacity. Non-motile epipsammic forms rely mostly on physiological mechanisms to optimize photoprotection capacity.

KEY WORDS: Microphytobenthos · Diatoms · Photoinactivation · Photoprotection · Repair · Vertical migration · Photoinhibition

INTRODUCTION

Photoprotection against photoinhibition has long been considered crucial for microphytobenthos (MPB) (Admiraal 1984, Kromkamp et al. 1998, Serôdio et al. 2001). These diatom-dominated communities inhabit intertidal and shallow subtidal sedimentary habitats of estuaries and coastal zones, characterized by highly dynamic and extreme abiotic conditions (Serôdio & Catarino 1999, Brotas et al. 2003, Chevalier et al. 2010). These include exposure to supersaturating solar irradiance during prolonged periods (Perkins et al. 2001, Laviale et al. 2015), extreme (high or low) temperature and salinity (Guarini et al. 1997, Serôdio et al. 2008), and nutrient and carbon limitation (Cook & Røy 2006, Vieira et al. 2016). Each of these factors and, more so, their combined effects are prone to cause a decrease in photosynthetic activity due to the photoinactivation of Photosystem II (PSII). Nevertheless, MPB sustain dense biofilms with high photosynthetic activity, and MPB primary productivity is ranked among the highest in marine

*Corresponding author: s.frankenbach@ua.pt

and estuarine ecosystems, matching or exceeding that of phytoplankton (Underwood & Kromkamp 1999).

The high productivity of MPB under extreme conditions has been thought to be enabled by particularly effective photoprotective mechanisms, allowing them to safely optimize the balance between light exposure and dissipation of excess absorbed light energy (Serôdio et al. 2012). In this context, the motility of benthic diatoms has long been considered to have an important photoprotective value. According to the 'behavioral photoprotection' hypothesis, the ability to vertically migrate within the photic zone of the sediment, covering a large range of light conditions in a short time, could enable motile diatoms to regulate light exposure and optimize photosynthesis while avoiding photodamaging irradiances (Admiraal 1984, Underwood et al. 1999, Consalvey et al. 2004). The photoregulatory nature of vertical migration is supported by increasing experimental evidence: (1) diatom motility is regulated by light intensity (Cohn et al. 2004, 2015, Serôdio et al. 2006, McLachlan et al. 2009); (2) biofilms treated with a motility inhibitor show a marked decrease in photosynthetic activity (Perkins et al. 2010, Serôdio et al. 2012); (3) high light-induced negative phototaxis is associated with susceptibility to photodamage (Ezequiel et al. 2015); and (4) light-induced migration is fast, occurring on time scales comparable to the activation of physiological photoprotection mechanisms (Laviale et al. 2016, Frankenbach & Serôdio 2017, Blommaert et al. 2018).

Motility-based photoprotection could operate complementarily to the physiological processes common to other photoautotrophs, the most important of which is considered to be the thermal dissipation of excessive light energy through the xanthophyll cycle (XC). In diatoms, the XC relies on the enzyme-mediated, reversible conversion of the PSII antenna pigment diadinoxanthin (DDx) into the energy-dissipation form diatoxanthin (DTx), which depends on the presence of a transthylakoidal proton gradient and on specific LHCx proteins (Blommaert et al. 2017, Lepetit et al. 2017). Compared to higher plants (Ruban et al. 2004), the XC of diatoms was found to operate in a particularly efficient way, especially in coastal and estuarine species (Lavaud 2007). The XC-related de-excitation of the antennae is often quantified by measuring the non-photochemical quenching (NPQ) of chlorophyll fluorescence (Müller et al. 2001, Ruban 2016). Because NPQ comprises several mechanisms of regulated energy dissipation in the PSII antenna, this fluorescence index has been widely used as a measure of photoprotective capacity of MPB (Jesus et al. 2006, Lavaud et al. 2007, Juneau et al. 2015).

A corollary of the 'behavioral photoprotection' hypothesis is the existence of a trade-off between motility-based and physiological photoprotective mechanisms: having the possibility to adjust light exposure behaviorally, motile species would rely less on physiological photoprotective processes, thus showing a decreased inherent photoprotective capacity (Serôdio et al. 2001, Barnett et al. 2015, Laviale et al. 2016). The replacement of the physiological photoprotection (at least partially) by motility is supported by the recent finding that high light-induced vertical migration is fast enough to allow the systematic avoidance of exposure to high light (Laviale et al. 2016, Frankenbach & Serôdio 2017), thus avoiding the development of a large physiological photoprotective capacity (Lavaud et al. 2007, Serôdio & Lavaud 2011, Barnett et al. 2015, Blommaert et al. 2018).

The relative importance of behavioral and physiological protection in MPB has been debated extensively in recent years (Serôdio et al. 2001, Van Leeuwe et al. 2008, Mouget et al. 2008, Pniewski et al. 2015, Barnett et al. 2015, Blommaert et al. 2017). This question has been often addressed by comparing 2 types of benthic diatom assemblages, taxonomically closely related and occurring virtually sympatrically (e.g. same tidal flat of the same estuary), but differing markedly regarding motility: the epipelon (EPL), formed by raphid motile species, dominant in fine sediments; and the epipsammon (EPM), composed predominantly of non-motile growth forms, common in coarser sediments, where they live in close association with sediment particles (Jesus et al. 2009, Cartaxana et al. 2011, Barnett et al. 2015, Juneau et al. 2015). The evidence gathered from the comparative study of EPL and EPM species appears to confirm the motility–physiology trade-off hypothesis, in the sense that motile forms tend to show a lower capacity for physiological photoprotection, either by having smaller cellular pools of energy-dissipating pigment DTx (Van Leeuwe et al. 2008, Jesus et al. 2009, Cartaxana et al. 2011, Pniewski et al. 2015) or by attaining lower maximum NPQ levels than their non-motile equivalents (Barnett et al. 2015, Blommaert et al. 2017, 2018, Pniewski et al. 2017).

The study of the photoprotective role of vertical migration and NPQ, and the trade-off between motility and physiological processes, has been based almost exclusively on the assessment of 'photoinhibition', defined in terms of net photoinactivation, that is, the decrease in photosynthetic activity resulting from the balance between PSII photoinactivation and

photorepair, without distinguishing their counteracting effects (e.g. Serôdio et al. 2012, Laviale et al. 2015). However, the evaluation of the actual photoprotective capacity provided by a certain process (e.g. vertical migration) is better attained by quantifying its effect in terms of the induced decrease of the susceptibility to photodamage (Serôdio et al. 2017). This in turn requires the separate quantification of the operation of PSII photoinactivation and repair processes, which can be adequately achieved by measuring the rate constants of inactivation and repair (k_{PI} and k_{REC}, respectively) and their responses to irradiance level (k_{PI} and k_{REC} versus E curves) (Murata et al. 2012, Campbell & Tyystjärvi 2012, Miyata et al. 2012).

This study addresses the comparative study of the inherent physiological photoprotection capacity of EPL and EPM diatom communities, directly testing the motility–physiology trade-off hypothesis based on actual PSII photoinactivation. The rate constant of photoinactivation, k_{PI}, and its variation with irradiance level, were used as a measure of the efficiency of photoprotection processes, testing the hypothesis that EPL species (when not using vertical migration) show a lower physiological photoprotection capacity, being more susceptible to photoinactivation (higher k_{PI}) than their EPM counterparts (lower k_{PI}). The study further intended to (1) test if the hypothesized lower inherent photoprotective capacity of motile species is compensated by a higher capacity for repair, (2) evaluate the effective photoprotective impact of XC-associated NPQ, and (3) characterize the relationship between NPQ and k_{PI}, evaluating the value of the NPQ index as a measure of photoprotection capacity.

Photoinactivation and repair processes were quantified in combination with the assessment of photoacclimation state and potential physiological photoprotection capacity, as conventionally measured by NPQ, taking advantage of a recently developed experimental approach allowing the high-throughput and integrated characterization of light responses and kinetics of photosynthetic samples (multi-actinic imaging fluorometry; Serôdio et al. 2017). The method is based on the combined use of imaging chlorophyll fluorometry and the simultaneous exposure of replicated samples to multiple actinic light levels and periods of exposure, allowing the rapid measurement of the induction and relaxation kinetics and of the light response of relative PSII electron transport rate (rETR; characterizing photoacclimation state) and NPQ (related to processes mediating photoprotection), and of the rate constants k_{PI} and k_{REC}.

MATERIALS AND METHODS

Sampling and sample preparation

Sediment samples were collected on 2 intertidal flats of the Ria de Aveiro, a mesotidal estuary located off the west coast of Portugal. The sampling sites were selected for their different distinctive characteristics regarding sediment granulometry and diatom species composition. Site Vista Alegre (40° 37′ 12″ N, 08° 44′ 54″ W) is composed of fine muddy sediments (97% particles <63 µm) and is expected to be dominated by EPL species, and will therefore be referred to as VA-EPL. Site Gafanha da Encarnação (40° 35′ 18″ N, 08° 41′ 06″ W) is composed of sandy mud (45.3% particles between 63 and 125 µm and 42.7% particles <63 µm) and is expected to be dominated by EPM species, and will therefore be referred to as GE-EPM. The tidal height of the 2 sampling sites is similar (ca. 2.3 m relative to hydrographic zero), with a mean duration of low tide (i.e. sediment exposure) of ca. 8 h 30 min (Serôdio et al. 2007). Sampling was carried out during August 2016, on 3 consecutive days for each site, when low tide took place during the middle of the day. The top 1 cm layer of the sediment was collected using a spatula and then transported to the laboratory, where it was sieved (1 mm mesh) and thoroughly mixed. The sediment was transferred into plastic trays to form a layer of 3–4 cm thick slurry and was maintained overnight immersed in natural seawater collected at the sampling site. The following day, before the start of the low-tide period, the overlying water was carefully removed, and cells were collected using the 'lens tissue' technique (Eaton & Moss 1966). Two layers of lens tissue (Lens cleaning tissue 105, Whatman) were placed on the surface of the sediment exposed to low white light (halogen lamps, 50 µmol photons m^{-2} s^{-1}) to induce upward migration of motile cells. After ca. 2 h, the upper piece of lens tissue was removed and microalgae were resuspended in filtered natural seawater, producing the cell suspensions used in the experiments.

Photoacclimation state and photoprotection capacity

The photoacclimation state and the potential photoprotection capacity of the samples was characterized by measuring light-response curves and induction kinetics of relative electron transport rate of PSII (rETR) and NPQ, respectively (see Table 1 for notation). rETR was determined by measuring chloro-

phyll fluorescence parameters F_s and F_m' on samples exposed to irradiance level E (Genty et al. 1989):

$$\mathrm{rETR} = E\,\frac{F_m' - F_s}{F_m'} \quad (1)$$

Because F_m' values measured under low light in MPB samples may be higher than the F_m value measured after dark-adaptation, NPQ was calculated using the adapted NPQ index, based on the relative difference between the maximum fluorescence level measured during the construction of the light-response or induction curves, $F_{m'm}$, and the level measured upon exposure to light, F_m' (Serôdio et al. 2008):

$$\mathrm{NPQ} = \frac{F_{m'm} - F_m'}{F_m'} \quad (2)$$

Table 1. Notation

α	Initial slope of the rETR versus E curve (μmol^{-1} m^2 s)
A	Fraction of functional PSII
AAL	Areas of actinic light
AOI	Areas of interest
DDx, DTx	Xanthophyll cycle pigments diadinoxanthin and diatoxanthin
E	PAR irradiance (μmol photons m^{-2} s^{-1})
E_k	Light-saturation parameter of the rETR versus E curve (μmol photons m^{-2} s^{-1})
E_{50}	Irradiance level corresponding to 50% of NPQ_m in an NPQ versus E curve
rETR	PSII relative electron transport rate
$rETR_m$	Maximum rETR in a rETR versus E curve
F_o, F_m	Minimum and maximum fluorescence of a dark-adapted sample
F_s, F_m'	Steady-state and maximum fluorescence of a light-adapted sample
F_v/F_m	Maximum quantum yield of PSII
k_{PI}, k_{REC}	Rate constants of photoinactivation and repair of PSII (s^{-1})
LC	Light-response curve
MPB	Microphytobenthos
NPQ	Non-photochemical quenching index
NPQ_m	Maximum NPQ value reached in a NPQ versus E curve
n	Sigmoidicity coefficient of the NPQ versus E curve
Φ_{PI}	Relative quantum yield of photoinactivation (m^2 μmol photons^{-1})
PSII	Photosystem II
T	Duration of light exposure for each irradiance E (min)
XC	Xanthophyll cycle

The light-response curves of rETR and NPQ were described by fitting the models of Eilers & Peeters (1988) and Serôdio & Lavaud (2011), respectively. rETR versus E curves were described by model parameters α (the initial slope of the curve), $rETR_m$ (maximum rETR) and E_k (the light-saturation parameter). NPQ versus E curves were described by model parameters NPQ_m (maximum NPQ), E_{50} (E corresponding to 50% of NPQ_m) and n (sigmoidicity parameter). Models were fitted and model parameters were estimated by iteratively minimizing a least-squares function, forward differencing, and the default quasi-Newton search method, using a procedure written in MS Visual Basic and based on MS Excel Solver.

Photoinactivation and repair

The rate constants of PSII photoinactivation and repair, k_{PI} and k_{REC}, were measured in the dark following exposure to actinic light. Rates were calculated under the assumptions that (1) the pool of functional PSII can be estimated by the maximum PSII quantum yield, calculated as $F_v/F_m = (F_m - F_o)/F_m$, (2) PSII photoinactivation and repair occur concurrently and can be described as 2 opposite first-order reactions, and (3) at the beginning of light exposure all PSII photosystems are functional (Kok 1956, Ni et al. 2017). In this case, the variation of net photoinactivation over time of exposure can be described by:

$$A(E,T) = \frac{k_{REC}(E) + k_{PI}(E)\mathrm{e}^{-(k_{PI(E)} + k_{REC(E)})T}}{k_{PI}(E) + k_{REC}(E)} \quad (3)$$

where A is the fraction of functional PSII, measured by the ratio of the $F_v/F_m(E,T)$ values measured after exposure to actinic light level E during a period T, and the initial, pre-stress F_v/F_m values (Campbell & Tyystjärvi 2012). $F_v/F_m(E,T)$ values were measured after 15 min of recovery in darkness. This time period has been used for MPB samples before, as it allows for the relaxation of the XC-associated NPQ (q_E), while preventing the build-up of significant sustained NPQ during prolonged darkness (Serôdio et al. 2012). The rate constants k_{PI} and k_{REC} were quantified for each E level as described by Campbell & Tyystjärvi (2012). k_{PI} was measured on samples treated with lincomycin (2 mM; lincomycin hydrochloride, Alfa Aesar; added in the dark 30 min before the start of the experiment), an inhibitor of the de novo synthesis of chloroplast-encoded proteins such as D1, by fitting the simplified form of Eq. (3) (setting $k_{REC} = 0$) to the time series of $A(E,T)$:

$$A(E,T) = e^{-k_{PI}(E)T} \quad (4)$$

k_{REC} was estimated by fitting Eq. (3) to the time series of A values measured in untreated samples and using the corresponding $k_{PI}(E)$ estimates.

The relative quantum yield of photoinactivation, Φ_{PI}, was determined from the slope of linear regression equation of k_{PI} against irradiance level E (Hakala et al. 2005):

$$\Phi_{PI} = \frac{k_{PI}(E)}{E} \quad (5)$$

Because Φ_{PI} measures directly the susceptibility to inactivation per incident photon, by integrating the effects of all protective mechanisms in operation, it is used in this study as an indicator of the global effectiveness of photoprotection.

In order to evaluate the contribution of XC-related NPQ, rate constants k_{PI} and k_{REC} (and their response to light: Φ_{PI} and k_{REC} versus E curve) were also measured in samples treated with nigericin (2.67 µM; nigericin sodium salt, Sigma-Aldrich), an uncoupler that relaxes the transthylakoidal ΔpH by antiporting H^+ and K^+, thus preventing the induction of the XC and related NPQ (Antal et al. 2011). On lincomycin-treated samples, pH was adjusted to 7.9 ± 0.1, using 1 M NaOH. Sodium bicarbonate ($NaHCO_3$, 4 mM, Sigma-Aldrich) was added to all samples before each experiment.

Multi-actinic imaging of chlorophyll fluorescence

All described fluorescence parameters and indices used to characterize the photoacclimation state, photoprotection capacity, photoinactivation and repair were measured in a single experiment, by applying the multi-actinic imaging fluorometry protocol described by Serôdio et al. (2017). This approach is based on the combined use of a digital light projector, as source of actinic light, and an imaging chlorophyll fluorescence system, allowing for the simultaneous measurement of the response of a large number of samples subjected to different combinations of light intensity (E) and exposure duration (T).

Actinic light was provided by an LCD digital projector (EB-X14; Seiko Epson), comprising one mercury arc lamp providing a maximum light output of 3000 lm. A 'light mask' consisting of a set of 64 circular, spatially separated areas of actinic light (AAL), arranged in an 8 × 8 matrix, was projected on a custom-made 3D-printed 64-well plate containing the samples (Serôdio et al. 2017), so that each AAL covered the whole surface of each sample. The light masks were designed in Microsoft PowerPoint, using a code written in Microsoft Visual Basic defining the number, position, size, shape, light intensity and spectrum (R:G:B ratios) of each individual AAL (Serôdio et al. 2013). The light spectrum was kept constant across light intensities by adjusting the RGB code for each intensity (Frankenbach & Serôdio 2017). Incident PAR irradiance was measured using a calibrated flat PAR sensor (mini quantum sensor LS-C and ULM-500 unit; Heinz Walz) at a distance from the light source that corresponded to the sample surface (bottom of the wells). The imaging fluorometer was a FluorCAM 800MF (Photon System Instruments, PSI), comprising a computer-operated control unit (SN-FC800-082, PSI) and a CCD camera (CCD381, PSI) with an f1.2 (2.8–6 mm) objective (Eneo). Four 13 × 13 cm LED panels emitting red light (emission peak at 621 nm, 40 nm bandwidth) provided modulated measuring light (<0.1 µmol photons m^{-2} s^{-1}) and saturating pulses (>7000 µmol photons m^{-2} s^{-1}, 0.8 s).

The experiments consisted of 3 phases. An initial period of 30 min of dark acclimation allowed cells to settle in the 64-well plates (working sample volume of 200 µl), after which reference values of F_v/F_m were measured. This was followed by an induction phase of exposure to actinic light, during which light-response curves and induction kinetics were measured by applying saturating pulses every 3.75 min; the samples were arranged in a square 8 × 8 matrix, in which each row corresponded to one of 8 actinic light levels (37, 135, 231, 352, 506, 692, 873 and 1120 µmol photons m^{-2} s^{-1}), and each column corresponded to one of 8 light exposure periods (T; 3.75 to 30 min). During the final recovery phase, samples were returned simultaneously to darkness and F_v/F_m was measured after 15 min to allow relaxation of XC-related NPQ. Because each experiment yielded only one estimate of k_{PI} and k_{REC} per E level, experiments were run 3 times on independent samples collected in each sampling date.

Image analysis and determination of fluorescence parameters

Images (512 × 512 pixels, 695–780 nm spectral range) of chlorophyll fluorescence parameters F_o, F_m (measured during dark-acclimation) or F_s and F_m' (measured during induction), were captured and processed using the FluorCam7 software (Photon Systems Instruments). For each measurement, 64 'areas of interest' (AOI) were designed as slightly

smaller than the corresponding AAL, to avoid misinterpretation due to border effects, having on average 186 pixels (5.8 mm diameter). The fluorescence parameters were measured by averaging all pixel values in each AOI, and by averaging the fluorescence intensity during the 2 s immediately before the saturating pulse (F_o, F_s) and during 0.8 s (F_m, F_m') exposure to the saturating pulse. Fluorescence images were captured at regular time intervals using an AutoHotKey script (www.autohotkey.com), written to automatically run the FluorCam7 protocol used for applying saturating pulses.

Chlorophyll *a* concentration

Chlorophyll *a* concentration of the suspensions was determined according to Lorenzen (1967). A 2 ml volume of the cell suspension was centrifuged and suspended in cold 90% acetone. Extraction was carried out overnight at 4°C. Samples were centrifuged (10 000 × *g*, 15 min), and the absorbance of the supernatant was measured spectrophotometrically (Spectronic Genesys 6 UV/VIS, Thermo Scientific) at 664 and 750 nm before and after addition of 10% HCl.

Taxonomic composition

Sub-samples of the cell suspensions were fixed in 1% v/v in Lugol's solution (5% Iodine, AppliChem) and viewed under a bright-field microscope for determination of the relative abundance of major taxonomic groups (diatoms, euglenophytes and cyanobacteria). Diatom identification was performed on sub-samples oxidized using concentrated nitric acid (1/4 v/v) and potassium permanganate. Permanent microscopy slides of the frustules were mounted using a high refractive index medium (Naphrax; Northern Biological Supplies). Composition of samples was determined by counting a minimum of 300 cells or valves on 3 replicated sub-samples, using a counting chamber (Neubauer-improved, Marienfeld). Diatom identification was based on Round et al. (1990), Ribeiro (2010), and Coste & Rosebery (2011).

Statistical analyses

Measurements under different treatments or times were compared by applying Student's *t*-test or one-way ANOVA. Assumptions of normality and homoscedasticity were verified prior to analysis using the Shapiro-Wilk test and Levene's test, respectively. In case of violation of assumptions, data were log transformed. Regression equations (slope and intercept) were compared by applying analysis of covariance (ANCOVA). All statistical analyses were carried out using Statistica 10 (StatSoft).

RESULTS

Sample taxonomic composition and chlorophyll content

The biofilms collected at the muddy site (VA-EPL) almost exclusively comprised diatoms (relative abundance 99.5%), being dominated by EPL forms of the genera *Stauroneis* (31%), *Navicula* (24%) and *Craticula* (23%), followed by the less abundant genera *Gyrosigma* (5.7%), *Nitzschia* (3.6%), *Amphora* (2.2%), *Paralibellus* (1.1%), *Anchanthes* (0.8%), *Gomphora* (0.6%), *Suriella* (0.4%) and *Diploneis* (0.2%). The biofilms of the sandy mud site (GE-EPM) had a lower relative abundance of diatoms (82% of total cell counts), and a higher occurrence of euglenophytes (13%) and cyanobacteria (0.2%). The diatom community was more diverse and dominated by EPM species of the genera *Navicula* (30%), *Amphora* (18%), *Achnanthes* (17%) and *Paralibellus* (14%), followed by *Gomphonema* (6.2%) and *Nitzschia* (5.8%). Least abundant were *Pinnularia* (1.2%), *Suriella* (1.1%), *Stauroneis* (1.0%), *Gomophycmbella* (0.9%), *Planothidium* (0.8%), *Cymbella* (0.7%), *Cylindrotheca* (0.5%), *Cocconeis* (0.3%), *Fallacia* (0.1%), *Plagiotropis* (0.1%) and *Ophera* (0.1%). The chlorophyll *a* content of VA-EPL and GE-EPM suspensions used in the experiments averaged 8.4 ± 0.5 and 2.2 ± 0.6 µg ml^{-1}, respectively.

Photoacclimation state and photoprotection capacity

The cell suspensions collected from the 2 habitats responded differently to increasing light intensity (Fig. 1). The samples from VA-EPL, dominated by EPL diatoms, showed a marked decrease in F_m' with increasing irradiance, down to less than 50% of the F_m value for the maximum applied irradiance (E = 1120 µmol photons m^{-2} s^{-1}) (Fig. 1A). For some samples, an increase of F_m' under low light (E < 210 µmol photons m^{-2} s^{-1}) was noticeable, reaching values above F_m, denoting the dissipation of NPQ formed in the dark (data not shown). In contrast, F_s increased

slightly under intermediate irradiances, reaching maximum values for E = 327 µmol photons m^{-2} s^{-1}, then decreasing to a minor extent (ca. 15%) under higher light levels, an indication of little limitation of photochemistry under high irradiance (Fig. 1A). Both F_m' and F_s remained relatively stable over time after 5–15 min of light exposure.

In contrast with the VA-EPL samples, the suspensions from the sandy mud site (GE-EPM) showed a smaller decrease of F_m' with increasing irradiance (only ca. 20%; Fig. 1B) during the first periods of light exposure, an indication of a more limited capacity for NPQ induction. Additionally, the light response of F_m' changed markedly over time, with F_m' values continuously decreasing after 7.5 min of light exposure (Fig. 1B). F_m' always decreased monotonically with E and there were no observations of $F_m' > F_m$, reflecting the absence of dark-induced NPQ. Also in contrast with VA-EPL, F_s increased markedly and continuously with irradiance, reaching values up to 160% of F_o for E = 506 µmol photons m^{-2} s^{-1}, after which point it remained relatively stable. The large increase of F_s with irradiance was gradually attenuated over time (from 167% of F_o at 3.75 min to only 115% of F_o after 26.25 min of light exposure; Fig. 1B), denoting a limited sink capacity for electrons under high light.

The samples from VA-EPL and GE-EPM also differed substantially regarding the light-response curves of rETR and NPQ (Fig. 2). In the case of VA-EPL, rETR versus E curves were characterized by higher $rETR_m$ values and by not showing saturation under the range of applied irradiances, resulting in relatively high values of α and $rETR_m$ at steady-

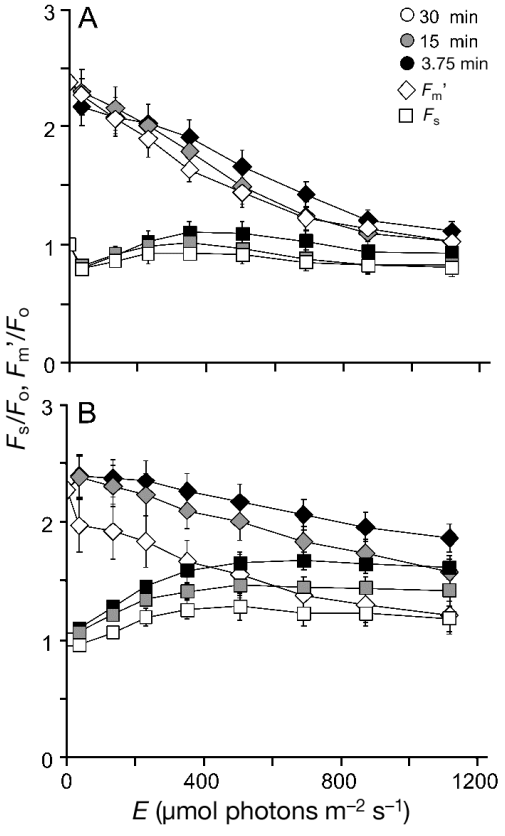

Fig. 1. Variation over time of light-response curves of fluorescence parameters F_s and F_m' (steady-state and maximum fluorescence of a light-adapted sample; normalized to F_o, minimum fluorescence of a dark-adapted sample) for samples collected at (A) VA-EPL and (B) GE-EPM sampling sites. E: irradiance. Light curves were measured at 3.75, 15 and 30 min after the start of light exposure. Data points are mean values of 9 replicated measurements. Error bars represent ±1 standard error

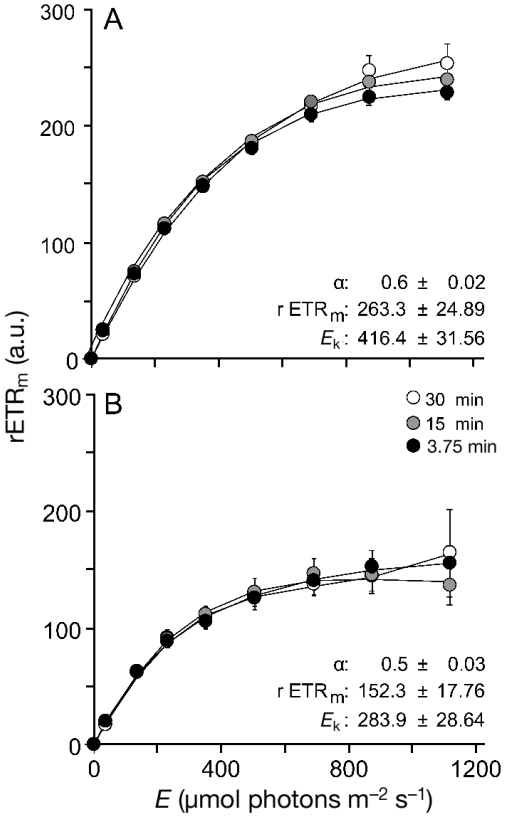

Fig. 2. Variation over time of light-response curves of relative electron transport rate at Photosystem II (rETR) for samples collected at (A) VA-EPL and (B) GE-EPM sampling sites. E: irradiance. Light curves were measured at 3.75, 15 and 30 min after the start of light exposure. Data points are mean values of 9 independent measurements. Error bars represent ± 1 standard error. Lines represent the model of Eilers & Peeters (1988) fitted to mean values at each time. Values of model parameters (α, $rETR_m$ and E_k) are given at the end of light exposure (30 min)

state and consequently high values of the photoacclimation parameter E_k (E_k = 416 µmol photons m^{-2} s^{-1}) (Fig. 2A). In contrast, light-response curves of rETR of GE-EPM samples showed a clear saturation, resulting in lower values of light curve parameters (E_k = 283 µmol photons m^{-2} s^{-1}) (Fig. 2B). In both cases, the rETR versus E curves did not change significantly during the exposure period and a steady state was reached within 30 min, although for the VA-EPL samples the rETR values varied more pronouncedly during the first 15 min of exposure (Fig. 2).

Concerning NPQ, VA-EPL and GE-EPM samples differed regarding the maximum values reached and the variation of the NPQ light response over time. For VA-EPL suspensions, NPQ increased with irradiance almost linearly, not reaching saturation under the applied irradiance levels (Fig. 3A). However, the NPQ light-response curves did not change substantially after 15 min of light exposure (Fig. 3C), suggesting that NPQ induction was fast and reached a steady state during the first minutes of light exposure. At steady-state, NPQ values measured under the highest E level reached around 1.2 while NPQ_m and E_{50} reached 2.7 and 1210 µmol photons m^{-2} s^{-1}, respectively. In contrast, GE-EPM samples reached lower maximum NPQ values (NPQ for the highest E < 0.6), although they continued to increase steadily during the whole period of light exposure, not showing signs of saturation.

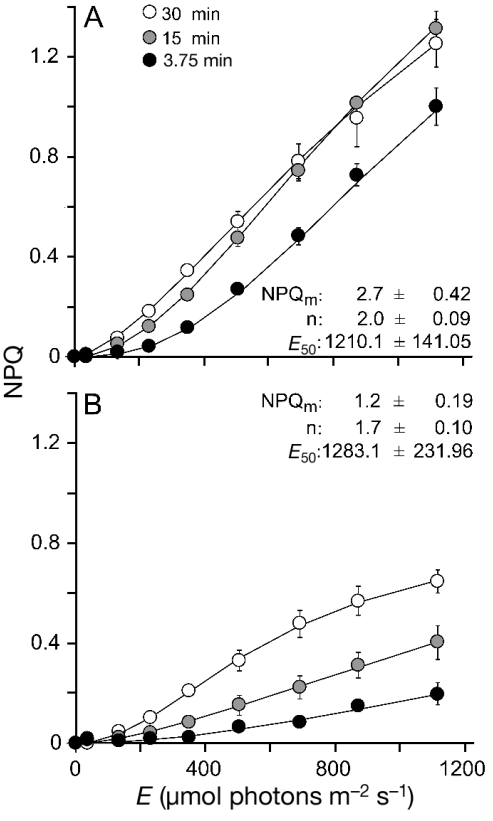

Fig. 3. Variation over time of light-response curves of non-photochemical quenching (NPQ) for samples collected at (A) VA-EPL and (B) GE-EPM sampling sites. E: irradiance. Light curves were measured at 3.75, 15 and 30 min after the start of light exposure. Data points are mean values of 9 independent measurements. Error bars represent ± 1 standard error. Lines represent the model of Serôdio & Lavaud (2011) fitted to mean values at each time. Values of model parameters (NPQ_m, n and E_{50}) are given at the end of light exposure (30 min)

Photoinactivation and repair

Fig. 4 illustrates the results obtained when measuring rate constants of photoinactivation and repair for a range of irradiance levels. These results refer to a single set of experiments carried out in a single day for each sampling site but are representative of all results. A striking feature of these results is that, in the case of VA-EPL samples exposed to low and intermediate light levels, A values did not decrease over time as expected but showed a transient increase to values above 1 during the first 10–20 min. Such an increase in F_v/F_m is compatible with the dissipation of NPQ formed in the dark prior to light exposure, and made it impractical to fit Eq. (3) and estimate k_{REC} for most of the light levels applied (E < 704 µmol photons m^{-2} s^{-1}). In GE-EPM samples, A did not increase over time as for VA-EPL, but remained relatively constant for the lower light levels. As a result, Eq. (3) could only be fitted, and k_{REC} estimated, for E > 349 µmol photons m^{-2} s^{-1} (Fig. 4B). Under high light levels, A reached lower values for the VA-EPL samples (0.75–0.8, for E = 1120 µmol photons m^{-2} s^{-1}) than for the GE-EPM samples (>0.9 for the same E), indicating a larger, slowly reversible component of NPQ.

On samples treated with lincomycin (L and L+N), A followed a well-defined negative exponential decay over time for most light levels, the rate of decay increasing with applied irradiance (Fig. 4, L, L+N). The same light- and time-response pattern was observed for VA-EPL and GE-EPM samples, although the rates of decrease were, for comparable E levels, noticeably lower for GE-EPM. In the case of GE-EPM samples, the fit of Eq. (4) resulted in the estimation of k_{PI} = 0 for several of the lowest light levels (E < 349 µmol photons m^{-2} s^{-1}) (Fig. 4B,

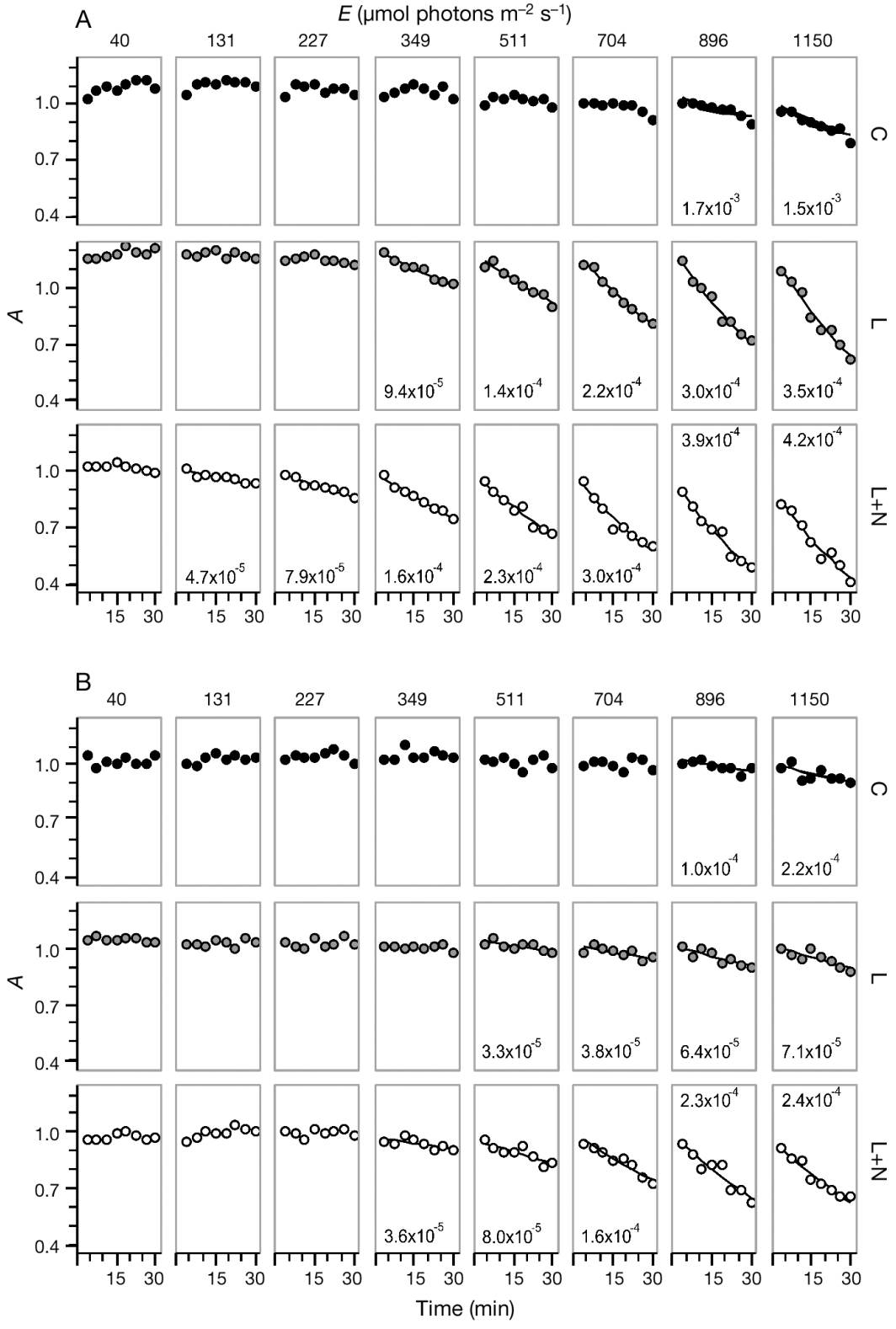

Fig. 4. Example of the variation with time of exposure of the fraction of functional Photosystem II (A) under different irradiance levels (E; values at the top), for controls (C), samples treated with lincomycin (L) and samples treated with lincomycin and nigericin (L+N). Results for samples collected at (A) VA-EPL and (B) GE-EPM (8 and 10 August 2016, respectively). Lines represent fitted models (Eqs. 3 & 4 for controls and lincomycin-treated samples, respectively) and numbers are the estimated rate constants (k_{REC} and k_{PI} for controls and lincomycin-treated samples, respectively)

L). Higher k_{PI} values were measured for VA-EPL samples, reaching up to 3.01 ± 0.15 × 10^{-4} s^{-1}, while for GE-EPM, maximum values reached only 1.10 ± 0.18 × 10^{-4} s^{-1} (average of all measurements). For both types of samples, the addition of nigericin caused an increase of the rate of decay of F_v/F_m. For VA-EPL samples, the addition of nigericin resulted in the complete elimination of the transient increase of *A*, possibly associated with the NPQ formed in the dark that was observed in the controls and in lincomycin-treated samples (Fig. 4A, L+N).

The availability of k_{PI} estimates for a wide range of irradiances allowed us to quantitatively describe its light response and to estimate the relative quantum yield of photoinactivation, Φ_{PI}. k_{PI} was found to increase linearly with *E* for both sampling sites and applied inhibitors (lincomycin and lincomycin + nigericin), as highly significant linear regressions were found in all cases ($p < 0.05$) (Fig. 5). In the case of VA-EPL samples treated with lincomycin, the absence of k_{PI} values for low light levels resulted in a positive *x*-intercept (*y*-intercept significantly different from zero; *t*-test, $t = -4.30$, df = 6, $p = 0.007$; Fig. 5). The slopes of the k_{PI} versus *E* linear regressions for lincomycin-treated samples, direct estimates of Φ_{PI}, were significantly higher for VA-EPL than for GE-EPM (Φ_{PI} = 3.25 × 10^{-7} and 1.27 × 10^{-7} m^2 µmol $photons^{-1}$ for VA-EPL and GE-EPM, respectively; ANCOVA, $F_{1,8} = 110.3$, $p < 0.001$). The addition of nigericin caused an increase of Φ_{PI} in both types of samples, but had a smaller effect in samples from VA-EPL than in those from GE-EPM (16.2% and 47.1%, respectively; Fig. 5). This increase was significant at the 5% significance level for both types of samples (ANCOVA, $F_{1,11}$ = 8.5, $p = 0.014$ and $F_{1,6} = 8.4$, $p = 0.027$ for VA-EPL and GE-EPM, respectively).

The relative importance of photoinactivation and repair processes can be assessed by comparing the rate constants and k_{PI} and k_{REC}. However, due to the lack of k_{REC} measurements for most of the *E* levels, the 2 rate constants were compared based on the values measured under the highest irradiance level alone (E = 1120 µmol photons m^{-2} s^{-1}) (Fig. 6). Repair rates were significantly higher for VA-EPL than for GE-EPM (17.1 and 2.4 × 10^{-4} s^{-1}, respectively; *t*-test, $t = 5.36$, df = 14, $p < 0.001$). More importantly, repair rates were considerably higher for VA-EPL than for GE-EPM when compared to the corresponding k_{PI} measurements, with the ratio k_{REC}/k_{PI} reaching 5.0 for VA-EPL but only 1.9 for GE-EPM samples.

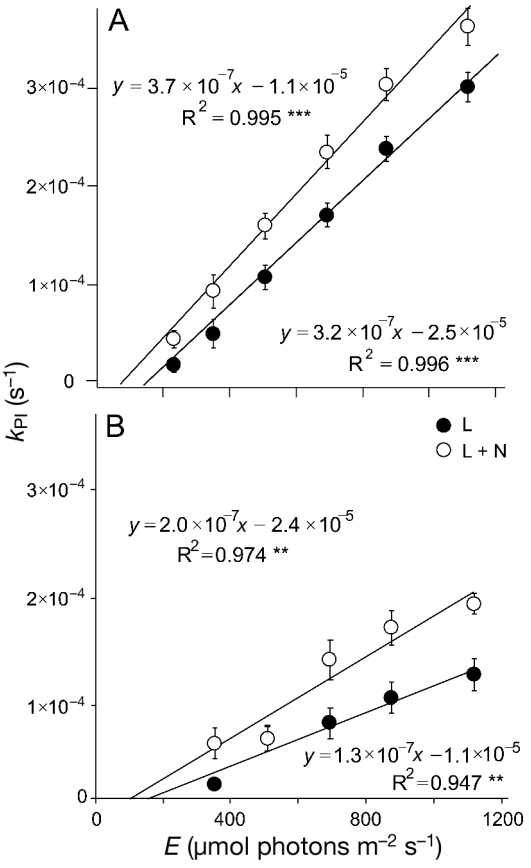

Fig. 5. Variation of the rate constants of photoinactivation (k_{PI}) with irradiance (*E*), as measured on samples treated with lincomycin (L) and with lincomycin and nigericin (L+N), for samples collected at (A) VA-EPL and (B) GE-EPM. Lines represent linear regression equations fitted to k_{PI} values. Data points are mean values of 9 replicated measurements. Error bars represent ±1 standard error. **p < 0.01; ***p < 0.001

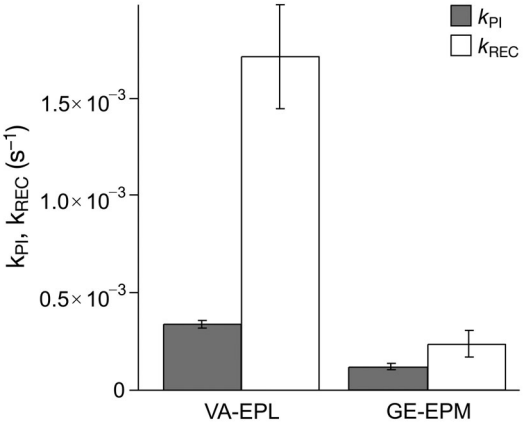

Fig. 6. Rate constants of photoinactivation (k_{PI}) and repair (k_{REC}) measured for the highest irradiance applied at each experiment (1120 µmol photons m^{-2} s^{-1}), for samples collected at VA-EPL and GE-EPM. Data points are mean values of 9 replicated measurements. Error bars represent ±1 standard error

DISCUSSION

Light response and induction kinetics of rETR and NPQ

The study of the motility–physiology trade-off hypothesis has been mostly based on the comparison of photophysiological properties related to photoprotection capacity of EPL and EPM species or communities. The observation of higher NPQ values (from light-response curves or light stress-recovery kinetics), larger XC pigment pools and de-epoxidation ratios in natural EPM assemblages (Van Leeuwe et al. 2008, Jesus et al. 2009, Pniewski et al. 2015), and non-motile species (Barnett et al. 2015, Juneau et al. 2015, Blommaert et al. 2017, 2018) has been interpreted as denoting a higher physiological photoprotective capacity to compensate for the lack of motility.

In what regards NPQ, the results of the present study seem to contradict this pattern. The EPL-dominated suspensions (VA-EPL) attained higher NPQ levels and greater rates of formation upon light exposure than the EPM-dominated suspensions (GE-EPM), which can be seen as an indication of a lower capacity of the non-motile cells to withstand the exposure to excess light. However, this apparent contradiction with the motility–physiology trade-off can be explained by the relatively small light doses applied in this study (maximum irradiance and exposure times lower than in most other studies), which may have prevented the observation of the full development of NPQ and limit the comparison between the EPL- and EPM-dominated samples. In fact, the results suggest that longer exposures could allow a different overall conclusion because, while for the VA-EPL samples NPQ remained constant at all light levels after the quick initial induction, the NPQ of GE-EPM samples continued to increase during the entire period of light exposure, making it likely that higher NPQ levels would be reached if longer incubations were applied.

Another explanation for the observed results is the possibility of latitudinal adaptation, as most of the cited studies were carried out at higher latitudes than the present study, and NPQ has been shown to be higher for MPB communities from higher latitudes (Laviale et al. 2015). However, the results of Jesus et al. (2009), showing higher XC pigment pool for EPM communities at lower latitudes, and of Pniewski et al. (2017, 2018), showing lower NPQ values for EPL communities at higher latitudes, do not support this hypothesis.

It must be mentioned that higher NPQ levels for EPL communities in comparison with EPM ones have also been reported by Pniewski et al. (2017, 2018). However, these studies compared MPB communities from rather distant and different habitats, factors that may have contributed to the observed differences.

These results are nevertheless ecophysiologically significant, informing on how the 2 types of communities deal with high light. EPL species seem capable of a fast activation of NPQ, presumably through the operation of the XC, but a limit in NPQ development, as its maximum is reached within only a few minutes. Thus, while the measured NPQ levels may be higher than for EPM samples (for the applied exposure times), EPL assemblages may in fact have a more limited protection capacity (Fig. 6). Motile cells might use NPQ to quickly respond to fast increases in irradiance, relying on vertical migration to adjust light exposure once the NPQ capacity is reached. In contrast, EPM species do not rely as much on a fast NPQ induction but are capable of maintaining a sustained increase of NPQ levels during long exposure periods. The continued increase of NPQ is consistent with the de novo synthesis of XC pigments, and in fact EPM species have also been shown to have a higher capacity for de novo synthesis than EPL species (Blommaert et al. 2017, 2018). This strategy is compatible with the idea that EPM cells, being limited in their capacity to regulate light exposure through vertical migration, rely on an enhanced photoprotective physiological processes to minimize the cumulative damaging effects of prolonged exposure to excess light.

EPL and EPM assemblages also differed regarding the light response and induction kinetics of rETR. The light-response curves measured in VA-EPL and GE-EPM suspensions were typical of samples photoacclimated to high and low light, respectively, with the former attaining higher α and $rETR_m$, and resulting higher values of the photoacclimation parameter E_k. The high- and low-light photoacclimation responses were also noticeable when analyzing the light response of the fluorescence parameters F_s and F_m', which indicated that VA-EPL samples were not as photochemically limited and had a larger electron sink capacity under high irradiances than the EPM equivalents. These results may seem unexpected considering the sedimentary light environment of the 2 sites and the motility of respective dominant species (Serôdio et al. 2007): the higher light attenuation and the steeper light gradients of the muddy site VA-EPL could be expected to favor low-light-acclimated cells, especially if they are able to move away from high

light; in contrast, the deeper penetration of light in the GE-EPM sediment and consequent exposure of cells with limited motility to higher light levels would favor the acclimation to high light. Nonetheless, high- and low-light acclimation of EPL and EPM natural assemblages or species, respectively, have been consistently reported (Cartaxana et al. 2011, Barnett et al. 2015, Juneau et al. 2015, Pniewski et al. 2017, 2018)

We hypothesize that the high-light acclimation pattern of EPL species results from the use of motility to search for relatively high light levels within the steep vertical light gradient of muddy sediments. While avoiding accumulation at the surface under very high light levels, a negative phototactic response demonstrated experimentally (Cohn et al. 2004, 2015, Serôdio et al. 2006, Du et al. 2012, Laviale et al. 2016), motile cells could accumulate at sub-surficial layers, being exposed to relatively high light levels, maximizing the use of available light and optimizing photosynthetic carbon fixation and growth. Acclimation to high light allows higher light-saturated photosynthetic rates, supporting higher growth rates, and improves dissipating excitation pressure within PSII through photochemistry, being of clear photoprotective value (Niyogi 1999, Ralph et al. 1999, Gévaert et al. 2003). It also permits the generation of ATP, which is of importance to support the energy-expensive removal of D1 from photoinactivated PSII and subsequent PSII repair (Allakhverdiev et al. 2005, Campbell et al. 2013), found to be particularly efficient in EPL-dominated samples (see below).

The clear differences between the 2 types of samples were observed despite the well-known selectivity of the 'lens tissue' sampling method for motile cells (Yang et al. 2010). The main potential consequence of this bias is the underrepresentation of non-motile EPM species in the GE-EPM samples, which could have led to an underestimation of the real differences between the 2 types of communities.

Susceptibility to photoinactivation

The observed difference between the rate constants of photoinactivation, and their light response, of VA-EPL and GE-EPM samples indicates that epipelic and epipsammic assemblages differ significantly regarding their susceptibility to photoinactivation. Epipelic-dominated samples showed, for comparable irradiances, consistently higher values of k_{PI}, supporting that motile species are inherently (i.e. when impeded from migrating, as in a suspension) more susceptible to photoinactivation than non-motile ones. The linearity between k_{PI} and E, indicative of a reciprocity between the damaging effects of light intensity and time of exposure (Tyystjärvi & Aro 1996, Kou et al. 2012), allows using the slope of the regression of k_{PI} on E, Φ_{PI}, as a measurement the actual susceptibility to inactivation per incident photon. Φ_{PI} depends only on the applied light dose, and can thus be used to directly compare results of experiments based on different experimental conditions (light intensity and exposure duration).

The finding of higher values of Φ_{PI} for epipelic cells than for epipsammic ones supports the postulated existence of a trade-off between photoprotective motility and photophysiology. In comparison to non-motile species, motile forms appear as having a diminished physiological capacity for minimizing photodamage, which under natural conditions (in the sedimentary microenvironment) could be compensated by migrating vertically across the photic zone of the sediment. Epipsammic species, on the other hand, not being able to behaviorally regulate light exposure and absorption, use physiological mechanisms providing an enhanced global photoprotection capacity.

The Φ_{PI} values measured in the present study are within the range of published values for natural diatom assemblages, which vary from 1.1×10^{-7} m^2 µmol photons^{-1} for epipelic MPB (Cartaxana et al. 2013) to 3.8×10^{-7} m^2 µmol photons^{-1} for sea ice diatom-dominated samples (Petrou et al. 2010). The former value is the only measurement available for benthic diatoms, and was estimated from the published value of the relative decrease in D1 protein content following light exposure, assuming a negative exponential decay with light dose. The fact that this value is lower than what was observed in the present study for epipelic samples, in spite of the fact that a larger light dose was applied (1500 µmol photons m^{-2} s^{-1}, 60 min), may be explained by the larger error expected from a single endpoint, or by the fact that the published estimate was based on D1 protein content, known to be less sensitive than fluorescence-based indicators, and that do not always correlate directly with F_v/F_m (Zsiros et al. 2006).

Photoprotective role of NPQ

The addition of nigericin caused an increase in Φ_{PI} in both VA-EPL and GE-EPM samples. Nigericin is an uncoupler of thylakoid membranes that dissipates the transthylakoidal ΔpH and has long been used for assessing the role of photoprotective NPQ in plants

(Park et al. 1996, Ware et al. 2015) and algae (Doege et al. 2000, Christa et al. 2017), including diatoms (Ting & Owens 1993, Grouneva et al. 2008). An increase in overall PSII photoinactivation (as measured by Φ_{PI}) resulting from the addition of nigericin is thus indicative of the operation of ΔpH-related photoprotective components of NPQ (energy-dependent quenching, q_E; Müller et al. 2001, Ruban 2016) likely including the XC. The comparison of the extent of increase in Φ_{PI} in EPL and EPM assemblages can therefore be used as a measure of the relative protective importance of NPQ/XC in the 2 sample types.

The significant nigericin-induced increase in Φ_{PI} that was observed for both VA-EPL and GE-EPM is an indication of an important photoprotective role of q_E and the XC in both types of communities. However, the larger increase in Φ_{PI} found for GE-EPM samples supports the idea that the XC displays a more important role in the EPM- than in the EPL-dominated assemblages. This result further supports the motility–physiology trade-off hypothesis. Non-motile species, incapable of using vertical migration to regulate light exposure, appear to rely more on efficient inherent physiological photoprotection. In contrast, the smaller increase in PSII photoinactivation in nigericin-inhibited VA-EPL samples shows that the importance of physiological mechanisms is smaller for motile species, which likely rely more on light-induced motility to photoprotect against excess light.

Interestingly, nigericin had the effect of eliminating the transient increase in F_v/F_m observed in VA-EPL samples (Fig. 4A), resulting in *x*-intercepts closer to zero (Fig. 5A). This result suggests that sustained NPQ formed in the dark may be related to the establishment and maintenance of a transthylakoidal ΔpH, as proposed for planktonic diatoms (Jakob et al. 2001, Dijkman & Kroon 2002, Bailleul et al. 2015). Because the sustained NPQ may also be caused by the permanence of DTx molecules in the dark, regardless of the presence of a transthylakoidal ΔpH (Lavaud & Lepetit 2013, Giovagnetti & Ruban 2017), the observed effect of nigericin might be due to changes in the activities of XC enzymes DT epoxidase and DD de-epoxidase.

The photoprotective role of motility and XC, and their relative importance, has been addressed in multiple studies. However, none has related the motility or the XC to the effective reduction in PSII photodamage, by distinguishing PSII photoinactivation from repair. An exception is the study by Cartaxana et al. (2013) that, by applying lincomycin and an inhibitor of the DDx–DTx cycle (dithiothreitol; Olaizola et al. 1994) on epipelic diatoms exposed to a single combination of light intensity and exposure duration, observed a large decrease (ca. −80 %) in D1 protein content, supporting a major role of the XC in preventing PSII photodamage. The results of the present study, based on the more robust indicator Φ_{PI}, pointed to a much lesser importance of physiological processes (Φ_{PI} increased by 16 and 47 % in EPL and EPM samples, respectively). The discrepancy between these results may be due to the different processes targeted by dithiothreitol and nigericin, but also to differences in photoacclimation state, associated with different growth conditions or differences in community composition, highlighting the need for further investigation of the variability of the responses to high light in natural MPB communities.

Photoinactivation versus repair

One advantage of the multi-actinic imaging protocol used in the present study is the possibility to measure paired light responses of rate constants k_{PI} and k_{REC}. However, specific aspects of the response of MPB samples under study limited the measurement of k_{REC} only for the highest applied irradiances. The absence of a clear decrease of F_v/F_m values for a large range of the lowest irradiances made it impossible to fit Eqs. (3) & (4) and to estimate k_{PI} and k_{REC}. The reasons for this differed between EPL and EPM samples. For VA-EPL samples (both untreated and treated with lincomycin), F_v/F_m increased transiently under the lower irradiances, a feature attributable to the build-up of sustained NPQ prior to light exposure. In the case of GE-EPM samples, a light-induced decrease in F_v/F_m of untreated samples was undetectable in most cases, which can be interpreted as resulting from an efficient coping with light under moderate conditions.

Nevertheless, the results regarding k_{PI} and k_{REC} for high light levels allowed for comparison of the relative importance of photoinactivation and repair processes, and point to different strategies of how EPL and EPM species respond to light stress. For both types of assemblages, the capacity of repair exceeds the suffered photodamage, even for the highest irradiance level tested. Yet, EPL forms appear to have the capacity for higher repair rates than EPM forms, the difference being especially relevant when considered in relation to the corresponding photoinactivation rates. EPL diatoms seem to rely more on repair than on preventing photoinactivation. They are inherently more susceptible to photodamage (higher Φ_{PI}), but this weaker photoprotective capacity is compensated

for by a greater capacity for repair, a strategy also observed in dinoflagellates (Jeans et al. 2013) and coccolithophorids (Ragni et al. 2008). This may explain why, despite showing higher rates of PSII photoinactivation, VA-EPL samples cope better with high light, showing higher light-saturated photosynthetic activity ($rETR_m$). Light-response strategies based on the development of efficient repair mechanisms tend to be favored by acclimation to high light (Ragni et al. 2008, Jeans et al. 2013). Repair capacity is known to increase with growth irradiance by improving the capacity to increase the rate of D1 protein synthesis (Tyystjärvi 2013). PSII repair is a costly process, and efficient use of high light levels, provided by high light acclimation, allows the generation of the necessary ATP and reductant power. Motile diatoms can make use of their motility to exploit the steep sedimentary light gradient and use the high light levels available near the surface in order to generate ATP and support the expensive D1 protein repair.

On the contrary, EPM forms seem to favor the reduction of photoinactivation, based on efficient physiological photoprotection, and thus avoiding the need to develop and support costly repair mechanisms. The inability to move within the photic zone of the sediment and to select a particular light environment leads EPM-dominated samples to appear, comparatively, as low-light acclimated.

The evaluation of the balance between susceptibility to photoinactivation versus repair capacity should also consider that diatoms, especially species with a limited capacity for photoprotective energy dissipation, seem to maintain a reservoir of inactive PSII as a means of favoring repair by providing additional substrate for PSII repair (Lavaud et al. 2016).

These results highlight the importance of measuring rate constants of photoinactivation and repair, and their light response, on MPB. It allows for the proper evaluation of the relative importance of the 2 processes in determining the level net photoinactivation of these communities across the range of ecologically relevant levels of light intensity, which is of interest to characterize their tolerance limits for light stress. The integrated study of photoprotection, photoinactivation and repair is also of interest in the context of the increasing experimental evidence indicating that the light stress acts predominantly by inhibiting repair and not by promoting inactivation (Nishiyama et al. 2006). This shift in paradigm has led to a growing interest in the study of photorepair, now seen as a key determinant of the effective capacity of phototrophs to cope with light stress (Murata et al. 2012).

Photoprotective capacity: NPQ versus Φ_{PI}

NPQ has been widely used as a measure of photoprotection capacity against photodamage in plants (e.g. Ruban et al. 2004) and algae (e.g. Gévaert et al. 2003, Barnett et al. 2015). In the case of MPB, NPQ (or the associated XC activity) has also been commonly used to ascertain the capacity for photoprotection. It has been used to compare the photoprotection capacity of EPL and EPM communities (XC pigment pools; Van Leeuwe et al. 2008, Cartaxana et al. 2011) or species (NPQ light response and induction/relaxation kinetics; Barnett et al. 2015, Blommaert et al. 2017) or to compare the fast induction of physiological (NPQ induction) and behavioral (negative phototaxis) photoprotection (Laviale et al. 2016). An important result of the present study was the finding that NPQ is not related to the capacity to prevent photodamage. In fact, the susceptibility to PSII photoinactivation, as measured by Φ_{PI}, varied markedly between EPL and EPM samples, but not as expected from the observed NPQ levels: VA-EPL samples reached higher NPQ levels, but were also the ones that suffered more photodamage; in contrast, GE-EPM samples were more resistant to PSII photoinactivation while reaching lower NPQ values. This contradiction between NPQ levels and actual photoinactivation suggests that NPQ may not be an accurate predictor of actual capacity to prevent photodamage, as it may not account for all photoprotective mechanisms at play, and its action may be complemented by other important protective processes, such as the PSII cyclic electron transfer (Lavaud 2007, Goss & Lepetit 2015), or by enhanced antioxidant activity (Nishiyama et al. 2006). Previous studies comparing NPQ with PSII photoinactivation have also concluded that NPQ offers a relatively low photoprotection, as little as 25% (e.g. Tyystjärvi 2013).

These results call for the use of Φ_{PI} (or k_{PI} for high light levels) instead of NPQ as a more suitable indicator of photoprotective capacity. Furthermore, particularly in the case of MPB biofilms, the measurement and use of NPQ has long been recognized as problematic, due to the sustained quenching in the dark of F_m values lower than F_m', and the confounding effects of light-induced vertical migration and light attenuation, and depth-integration of sub-surface fluorescence emission (Forster & Kromkamp 2004, Serôdio 2004, Morelle et al. 2018). In contrast, Φ_{PI} quantifies the total photodamage actually occurring without the confounding effects of NPQ and repair, integrating the effects of all protective mechanisms in operation, and therefore appears to be a better

predictor of the global effectiveness of photoprotection. Measuring Φ_{PI}, however, is considerably more difficult than measuring NPQ. Hopefully, the further development of experimental approaches such as the one used in the present study may overcome the current experimental limitations.

Acknowledgements. This work was supported by the Fundação para a Ciência e a Tecnologia (FCT), through doctoral scholarship SFRH/BD/86788/2012 (S.F.), Post-Doctoral fellowship SFRH/BPD/111685/2015 (J.C.F.) and CESAM grant UID/AMB/500017/2013 (W.S.). For the financial support, thanks are due to CESAM (UID/AMB/50017 – POCI-01-0145-FEDER-007638), FCT/MCTES through national funds (PIDDAC), and the co-funding by the FEDER, within the PT2020 Partnership Agreement and Compete 2020. The authors thank Gregor Christa for help with R programming, Sandra Craveiro, Carmen Elias and Ana Luís for help with the taxonomical identification, and Dr. Douglas A. Campbell for fruitful discussions on data interpretation. We thank anonymous reviewers for critical comments on the manuscript.

LITERATURE CITED

Admiraal W (1984) The ecology of estuarine sediment-inhabiting diatoms. Prog Phycol Res 3:269–322

Allakhverdiev SI, Nishiyama Y, Takahashi S, Miyairi S, Suzuki I, Murata N (2005) Systematic analysis of the relation of electron transport and ATP synthesis to the photodamage and repair of Photosystem II in *Synechocystis*. Plant Physiol 137:263–273

Antal TK, Osipov V, Matorin DN, Rubin AB (2011) Membrane potential is involved in regulation of photosynthetic reactions in the marine diatom *Thalassiosira weissflogii*. J Photochem Photobiol B 102:169–173

Bailleul B, Berne N, Murik O, Petroutsos D and others (2015) Energetic coupling between plastids and mitochondria drives CO_2 assimilation in diatoms. Nature 524:366–369

Barnett A, Méléder V, Blommaert L, Lepetit B and others (2015) Growth form defines physiological photoprotective capacity in intertidal benthic diatoms. ISME J 9: 32–45

Blommaert L, Huysman MJJ, Vyverman W, Lavaud J, Sabbe K (2017) Contrasting NPQ dynamics and xanthophyll cycling in a motile and a non-motile intertidal benthic diatom. Limnol Oceanogr 62:1466–1479

Blommaert L, Lavaud J, Vyverman W, Sabbe K (2018) Behavioural versus physiological photoprotection in epipelic and epipsammic benthic diatoms. Eur J Phycol 53: 146–155

Brotas V, Risgaard-Petersen L, Serôdio J, Ottossen L, Dalsgaard T, Ribeiro L (2003) In situ measurements of photosynthetic activity and respiration of intertidal benthic microalgal communities undergoing vertical migration. Ophelia 57:13–26

Campbell DA, Tyystjärvi E (2012) Parameterization of photosystem II photoinactivation and repair. Biochim Biophys Acta 1817:258–265

Campbell DA, Hossain Z, Cockshutt AM, Zhaxybayeva O, Wu H, Li G (2013) Photosystem II protein clearance and FtsH function in the diatom *Thalassiosira pseudonana*. Photosynth Res 115:43–54

Cartaxana P, Ruivo M, Hubas C, Davidson I, Serôdio J, Jesus B (2011) Physiological versus behavioral photoprotection in intertidal epipelic and epipsammic benthic diatom communities. J Exp Mar Biol Ecol 405:120–127

Cartaxana P, Domingues N, Cruz S, Jesus B, Laviale M, Serôdio J, Marques Da Silva J (2013) Photoinhibition in benthic diatom assemblages under light stress. Aquat Microb Ecol 70:87–92

Chevalier EM, Gévaert F, Créach A (2010) *In situ* photosynthetic activity and xanthophylls cycle development of undisturbed microphytobenthos in an intertidal mudflat. J Exp Mar Biol Ecol 385:44–49

Christa G, Cruz S, Jahns P, de Vries J and others (2017) Photoprotection in a monophyletic branch of chlorophyte algae is independent of energy-dependent quenching (qE). New Phytol 214:1132–1144

Cohn SA, Bahena M, Davis JT, Ragland RL, Rauschenberg CD, Smith BJ (2004) Characterisation of the diatom photophobic response to high irradiance. Diatom Res 19: 167–179

Cohn SA, Halpin D, Hawley N, Ismail A and others (2015) Comparative analysis of light-stimulated motility responses in three diatom species. Diatom Res 30:213–225

Consalvey M, Paterson DM, Underwood GJC (2004) The ups and downs of life in a benthic biofilm: Migration of benthic diatoms. Diatom Res 19:181–202

Cook PLM, Røy H (2006) Advective relief of CO_2 limitation in microphytobenthos in highly productive sandy sediments. Limnol Oceanogr 51:1594–1601

Coste M, Rosebery J (2011) Guide iconographique pour la mise en oeuvre de l'Indice Biologique Diatomée 2007. Action 14: Développement et optimisation des méthodes de bioindication pour les cours d'eau. Cestas Gazinet, Cemagref groupement de Bordeaux, Bordeaux

Dijkman NA, Kroon BMA (2002) Indications for chlororespiration in relation to light regime in the marine diatom *Thalassiosira weissflogii*. J Photochem Photobiol B 66: 179–187

Doege M, Ohmann E, Tschiersch H (2000) Chlorophyll fluorescence quenching in the alga *Euglena gracilis*. Photosynth Res 63:159–170

Du GY, Li WT, Li H, Chung IK (2012) Migratory responses of benthic diatoms to light and temperature monitored by chlorophyll fluorescence. J Plant Biol 55:159–164

Eaton JW, Moss B (1966) The estimation of numbers and pigment content in epipelic algal populations. Limnol Oceanogr 11:584–595

Eilers PHC, Peeters JCH (1988) A model for the relationship between light intensity and the rate of photosynthesis in phytoplankton. Ecol Modell 42:199–215

Ezequiel J, Laviale M, Frankenbach S, Cartaxana P, Serôdio J (2015) Photoacclimation state determines the photobehaviour of motile microalgae: the case of a benthic diatom. J Exp Mar Biol Ecol 468:11–20

Forster RM, Kromkamp JC (2004) Modelling the effects of chlorophyll fluorescence from subsurface layers on photosynthetic efficiency measurements in microphytobenthic algae. Mar Ecol Prog Ser 284:9–22

Frankenbach S, Serôdio J (2017) One pulse, one light curve: fast characterization of the light response of microphytobenthos biofilms using chlorophyll fluorescence. Limnol Oceanogr Methods 15:554–566

Genty B, Briantais JMM, Baker NR (1989) The relationship between the quantum yield of photosynthetic electron

transport and quenching of chlorophyll fluorescence. Biochim Biophys Acta 990:87–92

Gévaert F, Créach A, Davoult D, Migné A and others (2003) *Laminaria saccharina* photosynthesis measured *in situ*: photoinhibition and xanthophyll cycle during a tidal cycle. Mar Ecol Prog Ser 247:43–50

Giovagnetti V, Ruban A V. (2017) Detachment of the fucoxanthin chlorophyll a/c binding protein (FCP) antenna is not involved in the acclimative regulation of photoprotection in the pennate diatom *Phaeodactylum tricornutum*. Biochim Biophys Acta Bioenerg 1858:218–230

Goss R, Lepetit B (2015) Biodiversity of NPQ. J Plant Physiol 172:13–32

Grouneva I, Jakob T, Wilhelm C, Goss R (2008) A new multicomponent NPQ mechanism in the diatom *Cyclotella meneghiniana*. Plant Cell Physiol 49:1217–1225

Guarini JM, Blanchard GF, Gros P, Harrison SJ (1997) Modelling the mud surface temperature on intertidal flats to investigate the spatio-temporal dynamics of the benthic microalgal photosynthetic capacity. Mar Ecol Prog Ser 153:25–36

Hakala M, Tuominen I, Keränen M, Tyystjärvi T, Tyystjärvi E (2005) Evidence for the role of the oxygen-evolving manganese complex in photoinhibition of Photosystem II. Biochim Biophys Acta 1706:68–80

Jakob T, Goss R, Wilhelm C (2001) Unusual pH-dependence of diadinoxanthin de-epoxidase activation causes chlororespiratory induced accumulation of diatoxanthin in the diatom *Phaeodactylum tricornutum*. J Plant Physiol 158: 383–390

Jeans J, Campbell DA, Hoogenboom MO (2013) Increased reliance upon photosystem II repair following acclimation to high-light by coral-dinoflagellate symbioses. Photosynth Res 118:219–229

Jesus B, Perkins RG, Consalvey M, Brotas V, Paterson DM (2006) Effects of vertical migrations by benthic microalgae on fluorescence measurements of photophysiology. Mar Ecol Prog Ser 315:55–66

Jesus B, Brotas V, Ribeiro L, Mendes CR, Cartaxana P, Paterson DM (2009) Adaptations of microphytobenthos assemblages to sediment type and tidal position. Cont Shelf Res 29:1624–1634

Juneau P, Barnett A, Méléder V, Dupuy C, Lavaud J (2015) Combined effect of high light and high salinity on the regulation of photosynthesis in three diatom species belonging to the main growth forms of intertidal flat inhabiting microphytobenthos. J Exp Mar Biol Ecol 463: 95–104

Kok B (1956) On the inhibition of photosynthesis by intense light. Biochim Biophys Acta 21:234–244

Kou J, Oguchi R, Fan DY, Chow WS (2012) The time course of photoinactivation of photosystem II in leaves revisited. Photosynth Res 113:157–164

Kromkamp J, Barranguet C, Peene J (1998) Determination of microphytobenthos PSII quantum yield efficiency and photosynthetic activity by means of variable chlorophyll fluorescence. Mar Ecol Prog Ser 162:45–55

Lavaud J (2007) Fast regulation of photosynthesis in diatoms: mechanisms, evolution and ecophysiology. Funct Plant Sci Biotechnol 1:267–287

Lavaud J, Lepetit B (2013) An explanation for the inter-species variability of the photoprotective non-photochemical chlorophyll fluorescence quenching in diatoms. Biochim Biophys Acta Bioenerg 1827:294–302

Lavaud J, Strzepek RF, Kroth PG (2007) Photoprotection capacity differs among diatoms: Possible consequences on the spatial distribution of diatoms related to fluctuations in the underwater light climate. Limnol Oceanogr 52:1188–1194

Lavaud J, Six C, Campbell DA (2016) Photosystem II repair in marine diatoms with contrasting photophysiologies. Photosynth Res 127:189–199

Laviale M, Barnett A, Ezequiel J, Lepetit B and others (2015) Response of intertidal benthic microalgal biofilms to a coupled light-temperature stress: evidence for latitudinal adaptation along the Atlantic coast of Southern Europe. Environ Microbiol 17:3662–3677

Laviale M, Frankenbach S, Serôdio J (2016) The importance of being fast: comparative kinetics of vertical migration and non-photochemical quenching of benthic diatoms under light stress. Mar Biol 163:1–12

Lepetit B, Gélin G, Lepetit M, Sturm S and others (2017) The diatom *Phaeodactylum tricornutum* adjusts nonphotochemical fluorescence quenching capacity in response to dynamic light via fine-tuned Lhcx and xanthophyll cycle pigment synthesis. New Phytol 214:205–218

Lorenzen CJ (1967) Determination of chlorophyll and pheopigments: spectrophotometric equations. Limnol Oceanogr 12:343–346

McLachlan DH, Brownlee C, Taylor AR, Geider RJ, Underwood GJC (2009) Light-induced motile responses of the estuarine benthic diatoms *Navicula perminuta* and *Cylindrotheca closterium* (Bacillariophyceae). J Phycol 45:592–599

Miyata K, Noguchi K, Terashima I (2012) Cost and benefit of the repair of photodamaged photosystem II in spinach leaves: roles of acclimation to growth light. Photosynth Res 113:165–180

Morelle J, Orvain F, Claquin P (2018) A simple, user friendly tool to readjust raw PAM data from field measurements to avoid over- or underestimating of microphytobenthos photosynthetic parameters. J Exp Mar Biol Ecol 503: 136–146

Mouget J, Perkins R, Consalvey M, Lefebvre S (2008) Migration or photoacclimation to prevent high irradiance and UV-B damage in marine microphytobenthic communities. Aquat Microb Ecol 52:223–232

Müller P, Li XP, Niyogi KK (2001) Non-photochemical quenching. a response to excess light energy. Plant Physiol 125:1558–1566

Murata N, Allakhverdiev SI, Nishiyama Y (2012) The mechanism of photoinhibition in vivo: Re-evaluation of the roles of catalase, α-tocopherol, non-photochemical quenching, and electron transport. Biochim Biophys Acta Bioenerg 1817:1127–1133

Ni G, Zimbalatti G, Murphy CD, Barnett AB and others (2017) Arctic Micromonas uses protein pools and non-photochemical quenching to cope with temperature restrictions on Photosystem II protein turnover. Photosynth Res 131:203–220

Nishiyama Y, Allakhverdiev SI, Murata N (2006) A new paradigm for the action of reactive oxygen species in the photoinhibition of photosystem II. Biochim Biophys Acta Bioenerg 1757:742–749

Niyogi KK (1999) Photoprotection revisited: genetic and molecular approaches. Annu Rev Plant Physiol Plant Mol Biol 50:333–359

Olaizola M, Roche J, Kolber Z, Falkowski PG, La Roche J, Kolber Z, Falkowski PG (1994) Non-photochemical fluorescence quenching and the diadinoxanthin cycle in a

marine diatom. Photosynth Res 41:357–370
Park YI, Chow WS, Anderson JM, Hurry VM (1996) Differential susceptibility of Photosystem II to light stress in light-acclimated pea leaves depends on the capacity for photochemical and non-radiative dissipation of light. Plant Sci 115:137–149
Perkins RG, Underwood GJC, Brotas V, Snow GC, Jesus B, Ribeiro L (2001) Responses of microphytobenthos to light: primary production and carbohydrate allocation over an emersion period. Mar Ecol Prog Ser 223:101–112
Perkins RG, Lavaud J, Serôdio J, Mouget JL and others (2010) Vertical cell movement is a primary response of intertidal benthic biofilms to increasing light dose. Mar Ecol Prog Ser 416:93–103
Petrou K, Hill R, Brown CM, Campbell DA, Doblin MA, Ralph PJ (2010) Rapid photoprotection in sea-ice diatoms from the East Antarctic pack ice. Limnol Oceanogr 55: 1400–1407
Pniewski FF, Biskup P, Bubak I, Richard P, Latała A, Blanchard G (2015) Photo-regulation in microphytobenthos from intertidal mudflats and non-tidal coastal shallows. Estuar Coast Shelf Sci 152:153–161
Pniewski FF, Richard P, Latała A, Blanchard G (2017) Non-photochemical quenching in epipsammic and epipelic microalgal assemblages from two marine ecosystems. Cont Shelf Res 136:74–82
Pniewski FF, Richard P, Latała A, Blanchard G (2018) Long- and short-term photoacclimation in epipsammon from non-tidal coastal shallows compared to epipelon from intertidal mudflat. J Sea Res 136:1–9
Ragni M, Airs RL, Leonardos N, Geider RJ (2008) Photoinhibition of PSII in *Emiliania huxleyi* (Haptophyta) under high light stress: The roles of photoacclimation, photoprotection, and photorepair. J Phycol 44:670–683
Ralph PJ, Gademann R, Larkum AWD, Schreiber U (1999) *In situ* underwater measurements of photosynthetic activity of coral zooxanthellae and other reef-dwelling dinoflagellate endosymbionts. Mar Ecol Prog Ser 180:139–147
Ribeiro L (2010) Intertidal benthic diatoms of the Tagus estuary: taxonomic composition and spatial-temporal variation. PhD thesis, University of Lisbon
Round FE, Crawford RM, Mann D (1990) The diatoms — biology & morphology of the genera. Cambridge University Press, Cambridge
Ruban AV (2016) Nonphotochemical chlorophyll fluorescence quenching: mechanism and effectiveness in protecting plants from photodamage. Plant Physiol 170: 1903–1916
Ruban A, Lavaud J, Rousseau B, Guglielmi G, Horton P, Etienne AL (2004) The super-excess energy dissipation in diatom algae: comparative analysis with higher plants. Photosynth Res 82:165–175
Serôdio J (2004) Analysis of variable chlorophyll fluorescence in microphytobenthos assemblages: implications of the use of depth-integrated measurements. Aquat Microb Ecol 36:137–152
Serôdio J, Catarino F (1999) Fortnightly light and temperature variability in estuarine intertidal sediments and implications for microphytobenthos primary productivity. Aquat Ecol 33:235–241
Serôdio J, Lavaud J (2011) A model for describing the light response of the nonphotochemical quenching of chlorophyll fluorescence. Photosynth Res 108:61–76
Serôdio J, Marques da Silva J, Catarino F (2001) Use of *in vivo* chlorophyll *a* fluorescence to quantify short-term variations in the productive biomass of intertidal microphytobenthos. Mar Ecol Prog Ser 218:45–61
Serôdio J, Coelho H, Vieira S, Cruz S (2006) Microphytobenthos vertical migratory photoresponse as characterised by light-response curves of surface biomass. Estuar Coast Shelf Sci 68:547–556
Serôdio J, Vieira S, Barroso F (2007) Relationship of variable chlorophyll fluorescence indices to photosynthetic rates in microphytobenthos. Aquat Microb Ecol 49:71–85
Serôdio J, Vieira S, Cruz S (2008) Photosynthetic activity, photoprotection and photoinhibition in intertidal microphytobenthos as studied *in situ* using variable chlorophyll fluorescence. Cont Shelf Res 28:1363–1375
Serôdio J, Ezequiel J, Barnett A, Mouget JL, Méléder V, Laviale M, Lavaud J (2012) Efficiency of photoprotection in microphytobenthos: role of vertical migration and the xanthophyll cycle against photoinhibition. Aquat Microb Ecol 67:161–175
Serôdio J, Ezequiel J, Frommlet J, Laviale M, Lavaud J (2013) A Method for the rapid generation of nonsequential light-response curves of chlorophyll fluorescence. Plant Physiol 163:1089–1102
Serôdio J, Schmidt W, Frankenbach S (2017) A chlorophyll fluorescence-based method for the integrated characterization of the photophysiological response to light stress. J Exp Bot 68:1123–1135
Ting CS, Owens TG (1993) Photochemical and nonphotochemical fluorescence quenching processes in the diatom *Phaeodactylum tricornutum*. Plant Physiol 101: 1323–1330
Tyystjärvi E (2013) Photoinhibition of Photosystem II. Int Rev Cell Mol Biol 300:243–303
Tyystjärvi E, Aro EM (1996) The rate constant of photoinhibition, measured in lincomycin-treated leaves, is directly proportional to light intensity. Proc Natl Acad Sci USA 93:2213–2218
Underwood GJC, Kromkamp J (1999) Primary production by phytoplankton and microphytobenthos in estuaries. Adv Ecol Res 29:93–153
Underwood GJC, Nilsson C, Sundback K, Wulff A (1999) Short-term effects of UVB radiation on chlorophyll fluorescence, biomass, pigments, and carbohydrate fractions in a benthic diatom mat. J Phycol 35:656–666
Van Leeuwe MA, Brotas V, Consalvey M, Forster RM and others (2008) Photoacclimation in microphytobenthos and the role of xanthophyll pigments. Eur J Phycol 43: 123–132
Vieira S, Cartaxana P, Máguas C, Marques Da Silva J (2016) Photosynthesis in estuarine intertidal microphytobenthos is limited by inorganic carbon availability. Photosynth Res 128:85–92
Ware MA, Belgio E, Ruban AV (2015) Comparison of the protective effectiveness of NPQ in *Arabidopsis* plants deficient in PsbS protein and zeaxanthin. J Exp Bot 66: 1259–1270
Yang H, Flower RJ, Battarbee RW (2010) An improved coverslip method for investigating epipelic diatoms. Eur J Phycol 45:191–199
Zsiros O, Allakhverdiev SI, Higashi S, Watanabe M, Nishiyama Y, Murata N (2006) Very strong UV-A light temporally separates the photoinhibition of photosystem II into light-induced inactivation and repair. Biochim Biophys Acta Bioenerg 1757:123–129

Editorial responsibility: Steven Lohrenz, New Bedford, Massachusetts, USA

Submitted: January 23, 2018; Accepted: June 18, 2018
Proofs received from author(s): August 5, 2018